HHS Public Access

Author manuscript

Skeletal Radiol. Author manuscript; available in PMC 2022 March 01.

Published in final edited form as:

Skeletal Radiol. 2021 March ; 50(3): 521–529. doi:10.1007/s00256-020-03589-4.

Imaging features and clinical course of undifferentiated round cell sarcomas with CIC-DUX4 and BCOR-CCNB3 translocations

Emily J Brady, MD,
New York Presbyterian/Weill Cornell, Department of Radiology 525 East 68th St, Box 141, New York NY 10065

Meera Hameed, MD,
Memorial Sloan Kettering Cancer Center, Department of Pathology, 1275 York Ave, New York, NY 10065

William D. Tap, MD,
Memorial Sloan Kettering Cancer Center, Department of Medicine, 1275 York Ave, New York, NY 10065

Sinchun Hwang, MD
Memorial Sloan Kettering Cancer Center, Department of Radiology, 1275 York Ave, New York, NY 10065

Abstract

Objective: To describe the pre-treatment imaging features and clinical course of undifferentiated round cell sarcomas with CIC-DUX4 and BCOR-CCNB3 translocations.

Materials and Methods: In this retrospective study, several pre-treatment imaging features (tumor location, size, enhancement pattern, necrosis, flow voids, calcification, and FDG avidity) and the clinical course of patients were evaluated.

Results: In 12 patients with CIC-DUX4 sarcomas (median age, 24 years; range, 12–75), sarcomas were located in the soft tissue (n=10), bone (n=1), and lungs (n=1). On MRI, all 10 CIC-DUX4 sarcomas presented as a large necrotic mass (mean size 6.7 cm, range 2.3–11.3) with 100% demonstrating contrast enhancement, 60% showing flow voids, and 20% demonstrating fluid-fluid levels. On PET, the mean SUVmax was 13.2 (range, 8.5–18.1). Among 12 patients with follow-up, 3 died within a year of diagnosis. The most common site of metastases was the lungs (5/12). In 5 patients with BCOR-CCNB3 sarcomas (median age, 14 years; range, 2–17), sarcomas

corresponding author: 212-610-0854, Hwangs1@mskcc.org.

Conflict of Interest: The authors declare that they have no conflict of interest.

Ethical approval: All procedures performed in studies involving human participants were in accordance with the ethical standards of the institutional and/or national research committee and with the 1964 Helsinki declaration and its later amendments or comparable ethical standards. This article does not contain any studies with animals performed by any of the authors.

Informed consent: The requirement for informed consent was waived for this study.

were located in the spine (n=2), femur (n=1), tibia (n=1), and pelvis (n=1). On radiograph or CT, 2 were lytic; 3 were sclerotic. Soft tissue calcifications occurred in 40% of BCOR-CCNB3 sarcomas. On MRI, all 3 BCOR-CCNB3 tumors enhanced with 33% demonstrating flow voids and 66% exhibiting necrosis. On PET, the mean SUVmax was 6.3 (range 5.7–6.9).

Conclusion: CIC-DUX4 sarcomas often present as necrotic and hypermetabolic soft tissue masses while sarcomas with BCOR-CCNB3 translocations are vascular bone lesions with necrosis at imaging. CIC-DUX4 sarcomas are clinically more aggressive than BCOR-CCNB3 sarcomas.

Keywords

undifferentiated round cell sarcoma; MRI; CT; PET; CIC-DUX4; BCOR-CCNB3

Introduction

Small round cell sarcomas are a heterogeneous group of tumors of which Ewing sarcoma is the most prototypical. Recent molecular studies have identified four subgroups of undifferentiated round cell sarcomas which lack the genetic translocation of classic Ewing sarcoma despite their similar histologic appearance of uniform sheets of small round blue cells with scant cytoplasm (1). Two unique genetic rearrangements, CIC-DUX4 and BCOR-CCNB3, have emerged as the most common translocations (2, 3). While pathologically similar to Ewing sarcoma, and thus previously referred to as “Ewing-like sarcoma,” the 2020 WHO classification has included CIC-DUX4 and BCOR-CCNB3 sarcomas in the undifferentiated round cell sarcoma group until further research emerges to determine if these subtypes should represent distinct entities (4).

While CIC-DUX4 rearrangement remains a rare occurrence, it is the most frequent rearrangement within the undifferentiated round cell sarcoma family and represents a particularly aggressive sarcoma with a 5-year survival rate of 43% compared to 77% for Ewing sarcoma (2, 5). Unlike Ewing sarcomas, up to 90% of CIC-DUX4-expressing sarcomas arise in the soft tissues, evenly distributed between extremities and trunk or pelvis (2, 6). BCOR-CCNB3 is the second most frequently recognized rearrangement, accounting for 4% of undifferentiated round cell sarcomas (1). Clinically, BCOR-CCNB3 sarcomas closely resemble skeletal Ewing sarcomas and typically present in children and young adults with a median age of 15 years, arising from bone in 60% of cases (2). Compared to CIC-DUX4 sarcomas, BCOR-CCNB3 sarcomas have a better prognosis with a 5-year survival of 72% (7).

While CIC-DUX4 and BCOR-CCNB3 sarcomas are not recognized as distinct entities in the 2020 WHO classification, recent pathological and molecular studies have shown that they represent biologically distinct subgroups with different clinical outcomes (2). Despite this emerging data and their aggressive clinical course, particularly for CIC-DUX4 sarcomas, treatment options are limited, and they are typically treated with the same protocols as Ewing sarcoma. In addition, despite the difference in clinical prognosis of these emerging entities, there is scarce information regarding the imaging appearance of sarcomas with CIC-DUX4 and BCOR-CCNB3 rearrangement. Therefore, we intended to describe the

pre-treatment imaging features and clinical course of undifferentiated round cell sarcomas with CIC-DUX4 and BCOR-CCNB3 translocations.

Materials and Methods

Patients

This retrospective study was approved by the institutional review board at Memorial Sloan Kettering Cancer Center and the requirement for informed consent was waived. The inclusion criteria included pathologically confirmed cases with available cross-sectional imaging for review in our institutional Picture Archiving and Communication System (PACS). We searched pathology reports at our institution for the diagnosis of “CIC-DUX4” or “BCOR-CCNB3” from January 2000 to December 2019, consequently identifying 12 patients with a diagnosis of CIC-DUX4 and 5 patients with a diagnosis of BCOR-CCNB3 with imaging available for review. Histology and pathology were reviewed by a pathologist on this study with more than 25 years of experience for confirmation of the diagnosis and patient inclusion into the study. Both CIC-DUX4 and BCOR-CCNB3 translocations were confirmed by florescence in situ hybridization (FISH) or targeted RNA sequencing analysis. Characteristic histologic appearance additionally aided in the diagnosis. Immunohistochemistry was used primarily to exclude other round cell tumors, such as lymphoma or rhabdomyosarcoma. Ewing sarcoma was excluded by negative EWSR1 translocation.

Pre-Treatment Imaging Review

All available pre-treatment imaging including radiography, CT, MRI, and PET/CT (^{18}F-Fluorodeoxyglucose Positron Emission Tomography) were reviewed in PACS by a musculoskeletal radiologist with 15 years of experience. We included all pre-treatment imaging whether they were performed at our institution or at an outside institution. All CT examinations were performed with intravenous contrast. All MRI examinations consisted of multiplanar imaging including T1-weighted sequence and fluid sensitive sequences as well as pre- and post-contrast T1-weighted images. All PET examinations used ^{18}F-Fluorodeoxyglucose as the standard radiotracer in combination with CT images for anatomic localization.

CIC-DUX4 primary tumors were assessed in terms of tumor location, site of origin, and size. On MRI, the following imaging features were specifically assessed: presence of contrast enhancement, necrosis, hemorrhage, perilesional edema, vascularity, and fluid-fluid levels. MRI contrast enhancement was further classified as $< 50\%$ of the tumor, $\geq 50\%$ of the tumor, or peripheral enhancement only. Perilesional edema at MRI was also further characterized as minimal, less in extent than the size of the overall tumor, or greater in extent than the size of the tumor. The tumor was considered vascular when multiple coursing vessels with flow voids were identified traversing the lesion. On CT, the presence of erosion of adjacent osseous structures or soft tissue calcifications as well as attenuation in comparison to skeletal muscle were assessed. On FDG-PET, the mean maximum standard uptake value (mean SUVmax) was assessed.

BCOR-CCNB3 primary tumors were described in terms of their location, site of origin, and size. On pre-treatment radiographs/CT, the following features were specifically assessed: lytic or sclerotic appearance, presence of periosteal reaction, and soft tissue calcifications. On MRI, signal on fluid-sensitive sequences, contrast enhancement, necrosis, perilesional edema, and vascularity were examined. In regard to enhancement, vascularity, and perilesional edema, similar classifications were used in BCOR-CCNB3 tumors as were used in CIC-DUX4 tumors. On FDG-PET, mean SUVmax was assessed.

Clinical Course Review

The medical record was reviewed for each patient to determine their clinical course, including chemotherapy, surgery, and radiation, as well as development of metastatic disease, length of follow-up, and death. Metastatic disease was confirmed either histologically or radiologically (if typical findings of metastases were seen on CT, MRI, or PET/CT).

Results

Imaging Characteristics of Undifferentiated Round Cell Sarcomas with CIC-DUX4 Genetic Translocations

Twelve patients were confirmed by pathology to have CIC-DUX4 positive sarcomas, with the first case identified in 2014. The median age of this patient group was 24 years (range 12–75). The sex distribution was 6 male and 6 female patients. Ten out of 12 (83%) sarcomas were soft tissue based: 3 were in subcutaneous tissue, 1 was in both subcutaneous and deep tissues, and 6 were in deep tissue. One (8%) sarcoma arose from bone, and one (8%) sarcoma arose from lung parenchyma. The average tumor size was 6.7 cm (range, 2.3–11.3). Of the 12 sarcomas, 3 were primary sarcomas of the trunk, 3 were of the pelvis, 3 were of the lower extremity, 1 was of the upper extremity, 1 was of the scalp, and 1 was of the lung.

Pre-treatment imaging was available for 11/12 patients with 10 MRI, 7 CT, and 5 PET examinations available for review (Table 1).

On pre-treatment MRI, all 10 sarcomas showed well-defined borders with heterogenous contrast enhancement with areas of non-enhancement suggestive of necrosis (Figs. 1–2). Perilesional edema was seen in 8/10 (80%) sarcomas. The majority of sarcomas (7/10, 70%) showed contrast enhancement in ≥ 50% of the tumor while 2/10 showed enhancement in < 50% and one tumor demonstrated only peripheral contrast enhancement. Prominent vascularity as evidence by flow voids were seen in 6/10 (60%) sarcomas (Figs 1–2). Less common features included the presence of fluid levels, which were seen in 2/10 (20%) sarcomas, and hemorrhage, which was seen in 5/10 sarcomas (50%) (Figs 3–4).

On pre-treatment CT, all 7 sarcomas demonstrated attenuation isodense or hypodense to skeletal muscle with heterogeneous enhancement. Erosions of adjacent osseous structures was identified in 2/7 (29%) patients. Calcifications were not identified in any of the pre-treatment tumors.

On pre-treatment PET, all 5 sarcomas were FDG-avid and the mean SUVmax was 13.2 (range, 8.5–18.1) (Figs. 1, 4–5). Heterogeneous uptake was seen in all patients.

Information regarding treatment course was obtained for 11/12 of the patients with CIC-DUX4 tumors with the remaining patient representing a consult patient who was not treated at our institution. Ten out of 11 patients underwent chemotherapy with an Ewing sarcoma type protocol which included doxorubicin, vincristine, cyclophosphamide, ifosfamide, and etoposide; one patient was initially misdiagnosed as having a small cell carcinoma of the lung and underwent one cycle of etoposide and carboplatin before discontinuing treatment. Eight out of 11 patients underwent resection of the primary tumor. Six out of 11 patients additionally underwent external beam radiation.

At the time of presentation, 3/12 (25%) patients had evidence of metastatic disease. An additional 3 patients developed metastatic disease at some point in their clinical course while six remained without evidence of distant metastases. The most common sites of metastatic disease were the lung (5/12), adrenal (3/12), lymph nodes (3/12) and brain (2/12); one patient developed metastatic disease in the pancreas, kidneys, lymph nodes, and bone (Fig. 4). Two patients developed local recurrence.

The mean follow-up period was 23 months (range 4–48). Of the 12 patients with CIC-DUX4 positive sarcomas at our institution, three (25%) died, ranging from within 4–19 months of initial presentation. Another three patients were lost to follow-up and at the time of their last clinical follow-up, two had lung metastases and another had no recurrent or metastatic disease. Of the remaining 6 patients, four are alive without evidence of disease and two are alive and living with multiple sites of metastatic disease.

Imaging Characteristics of Undifferentiated Round Cell Sarcomas with BCOR-CCNB3 Genetic Translocations

Five patients with histologically confirmed BCOR-CCNB3 positive sarcomas were identified. The first BCOR-CCNB3 positive tumor was identified in 2013. The median age of these patients was 14 years old (range 2–17 years) with male patients outnumbering female patients four to one. All 5 sarcomas appeared to arise from bone with a prominent extra-osseous soft tissue component: 1 arose in the lumbar spine, 1 in the thoracic spine, 1 in the femur, 1 in the tibia, and 1 in the pelvis. Of the tumors that originated in long bones, both arose eccentrically in the metadiaphysis with involvement of the medullary canal. Both spinal tumors arose from the vertebral bodies with one extending posteriorly into the spinal canal and the other extending anteriorly into the paraspinal musculature. The pelvic tumor arose from the iliac fossa. The average tumor size was 10.3 cm (range, 3.8–25.0).

Pre-treatment imaging included CT or radiograph available for 5 patients, MRI for 3 patients, and PET for 3 patients (Table 2).

On pre-treatment CT or radiograph, 2/5 (40%) sarcomas were predominately lytic while 3/5 (60%) sarcomas were predominately sclerotic (Figs. 6–7). The lytic lesions all demonstrated a permeative destructive appearance, consistent with Lodwick type 3 change (8). All sarcomas demonstrated a wide zone of transition and resulted in some degree of periosteal

reaction, often aggressive in appearance with either lamellated or sunburst appearance. Calcifications within the extra-osseous soft tissue component was seen in 2/5 (40%) of sarcomas (Fig. 7).

On pre-treatment MRI, 3/3 sarcomas demonstrated heterogeneously high signal on fluid sensitive sequences and avid contrast enhancement, with ≥ 50% of the tumor enhancing (Fig 6, 7). Flow voids were seen in 1/3 (33%) sarcomas while necrosis was seen in 2/3 (66%) sarcomas. Perilesional edema was identified in 2/3 (66%) sarcomas. Hemorrhage was not identified in any of the pre-treatment tumors.

On pre-treatment PET, metabolic activity was seen in 2/3 sarcomas, while 1 sarcoma was not FDG avid. For the 2 FDG-avid tumors, the mean SUVmax was 6.3 (range, 5.7–6.9).

Clinically, all five patients underwent resection of their primary tumors and four out of five patients completed chemotherapy, with doxorubicin, vincristine, cyclophosphamide, ifosfamide, and etoposide. One patient additionally received vindesin, cisplatin, and epirubicin in another country. The remaining patient is preparing to undergo additional treatment after recent surgical resection. No patients underwent radiation to their primary site.

The mean follow-up was 22.4 months (range, 2–41). While no patient was metastatic at the time of presentation, one patient developed metastases to the abdomen with development of a large subdiaphragmatic mass. This recurrence occurred approximately 40 months after presentation and resulted in death one month later. Of the remaining four patients, three are currently alive without evidence of recurrent or metastatic disease. The remaining one patient has undergone resection of his primary tumor and is preparing to initiate further treatment.

Discussion

While CIC-DUX4 and BCOR-CCNB3 positive sarcomas are molecularly distinct subtypes within the undifferentiated sarcoma family of tumors, and despite the small number of cases in our study, we found clinical and radiologic similarities between these sarcomas and Ewing sarcoma, as previously described in the literature (1–3, 5–7, 9–12).

Demographically, BCOR-CCNB3 patients in our study presented at a median age of 14 years; Ewing sarcoma patients classically presents at a median age of 15 years, with the majority of patients presenting within the first two decades of life (9, 12). CIC-DEIX4 patients in our study tended to present later in life, with a median age of 24 years and a wider age range, similar to extraskeletal Ewing sarcoma patients who tend to present later in life (19.5 years old) than skeletal Ewing skeletal patients. The median ages of patients with BCOR-CCNB3 and CIC-DUX4 sarcomas in our cohort are similar to those of previous studies (3, 6).

In our study, the location of the primary CIC-DUX4 sarcoma is similar to that of extraskeletal Ewing sarcoma as reported in the literature. Specifically, 50% of CIC-DUX4 sarcomas in our study arose in the trunk or pelvis and 33% arose in the upper or lower

extremity, which is reflective of the literature of extraskeletal Ewing sarcoma where tumors have been reported to arise in the trunk or pelvis (48–54%) and extremities (26–30%) (13–16). Meanwhile, the location of BCOR-CCNB3 sarcoma in our study was contrary to that of skeletal Ewing sarcoma in the literature. Here, 40% of BCOR-CCNB3 sarcomas in our study arose from the spine with the remainder (60%) arising from the pelvis and lower extremity long bones, while in the literature, Ewing sarcoma tumors are more frequently reported to arise from the pelvis (19-21%) and long bones of the lower extremity (30-44%) than in the spine (11%) (14, 17, 18). However, due to our small size of cases, this comparison of skeletal distribution is limited. Puls et al. reported that all 7 cases of bone BCOR-CCNB3 sarcomas in their study of 10 patients arose from the appendicular skeleton (6).

We note that CIC-DUX4 sarcoma shares many overlapping imaging features with extraskeletal Ewing sarcoma. However, a few distinctive features may assist in differentiating these two entities as suggested by our study (Table 3). While both sarcoma types tend to be isodense to hypodense to skeletal muscle on CT and display strong, heterogeneous enhancement (13, 14, 19), as seen in our study, no CIC-DUX4 sarcoma displayed calcifications while intra-tumoral calcifications have been reported in 0–25% of extraskeletal Ewing sarcoma (13, 14, 19). We hypothesize that CIC-DUX4 tumors in our study did not display calcifications as the majority in our study arose from soft tissues and thus did not include either osseous matrix formation or sequestered bone like many primary bone lesions. However, the lack of dystrophic calcifications remains difficult to explain; we speculate that a high rate of tumor growth might prevent the accumulation of calcifications within tumors. On PET, CIC-DUX4 sarcomas in our study displayed FDG avidity with an average SUVmax of 13.2, which is stronger than the reported SUVmax of 5–7 for extraskeletal Ewing sarcoma (13, 20). Several studies have shown that higher SUVmax is correlated with poorer outcomes in Ewing sarcoma, which may reflect the often worse clinical outcomes in patient with CIC-DUX4 sarcoma. On MRI, both CIC-DUX4 and extraskeletal Ewing sarcomas are likely to show heterogeneous contrast enhancement, though this was seen in 100% of CIC-DUX4 sarcomas in our study compared with 73.7–100% of extraskeletal Ewing sarcomas in the literature (13, 14, 21). Necrosis was common in both tumor types, contributing to the degree of heterogeneous enhancement. While hemorrhage was seen in 50% of CIC-DUX4 sarcomas with MRI in our study, Somarouthu et al. reported that 19% of extraskeletal Ewing sarcomas in their study demonstrated hemorrhage (13). Fluid levels were seen in 20% in our patients, probably due to hemorrhage or necrosis. While extraskeletal Ewing sarcoma is more likely to demonstrate high flow vascular channels, up to 90% in the literature versus 60% of CIC-DUX4 sarcomas on MRI in our study, vascular flow voids are also not unique to extraskeletal Ewing sarcoma and are seen in many high grade tumors including hemangioendotheliomas, hemangiopericytomas, angiosarcoma, and synovial sarcoma (14, 22).

In addition, we also note that BCOR-CCNB3 sarcoma exhibits similar imaging characteristics to skeletal Ewing sarcomas as previously reported (2). As shown in our study, radiographically, BCOR-CCNB3 sarcoma appears to be close to evenly distributed between predominately lytic and predominately sclerotic tumors, which is similar to skeletal Ewing sarcoma which has reported rates of sclerosis ranging from 32–40% (9,

14). BCOR-CCNB3 tumors in our study demonstrated a permeative appearance with a wide zone of transition. While this aggressive appearance is similar to the majority of cases of BCOR-CCNB3 tumors as well as skeletal Ewing sarcoma cases in the literature (76%–82%), there have been case reports of BCOR-CCNB3 lesions demonstrating a more benign appearance with geographic margins (14, 23). While periosteal reaction was seen in all BCOR-CCNB3 sarcomas in our study, it was reported in 58–84% of skeletal Ewing sarcomas in the literature (14). Calcifications were present in 40% of BCOR-CCNB3 sarcomas in our study compared to 7–9% of skeletal Ewing sarcomas in the literature (14, 18). On MRI, all BCOR-CCNB3 sarcomas displayed a heterogeneous signal, while 73% of skeletal Ewing sarcomas are typically homogeneous in appearance on MRI (12). Avid contrast enhancement is common in both BCOR-CCNB3 sarcomas and Ewing sarcomas. BCOR-CCNB3 sarcomas in our study frequently demonstrated internal necrosis which is also demonstrated in skeletal Ewing sarcoma in the literature, though more commonly in the pre-treatment setting (14, 24).

In terms of metastatic spread of CIC-DUX4 sarcomas, in our study, lungs were the most common site of metastasis, similar to extraskeletal Ewing sarcomas (3, 6, 9, 17, 25). In our BCOR-CCNB3 sarcoma population, only one patient developed intra-abdominal metastasis while skeletal Ewing sarcoma metastasizes in 26–28% of patients, typically to lung or bone (9, 25). Puls et al. reported that 4/10 patients with BCOR-CCNB3 sarcomas had lung metastases at initial diagnosis but found no association with overall survival, unlike Ewing sarcoma that shows significantly shorter overall survival when presenting with metastases (6). These findings and our infrequent rate of metastases may suggest less aggressive clinical course and better survival for patients with BCOR-CCNB3 than those with Ewing sarcoma.

The treatment of CIC-DUX4 and BCOR-CCNB3 tumors require a multidisciplinary approach, involving oncologists, surgeons, pathologists, radiologists, and radiation oncologists. The treatment protocol is similar to those of Ewing sarcoma, with most patients receiving chemotherapy, surgery and occasionally radiation therapy (26). However, recent studies suggest that CIC-DUX4 tumors in particular exhibit lower sensitivity to classic Ewing sarcoma treatment regimens (1). Our study echoes this point as 3/8 patients with CIC-DUX4 sarcomas during follow-up developed metastatic disease despite surgical resection and chemotherapy. BCOR-CCNB3 sarcomas, in contradistinction, are reported to be more chemosensitive to classic Ewing sarcoma treatment regimens. In one study, ten out of twelve patients demonstrated less than 10% viable tumor after chemotherapy (2). The 5-year overall survival for BCOR-CCNB3 sarcomas is reported as 75% which is similar to that seen in Ewing sarcoma cohorts (7, 10). In our study, only 1/5 patients developed metastatic disease after chemotherapy. Despite the growing consensus that CIC-DUX4 and BCOR-CCNB3 tumors are distinct tumors molecularly, until more research is done, therapy is likely to remain similar to that of classic Ewing sarcoma regimens.

Our study has several limitations. Because CIC-DUX4 and BCOR-CCNB3 sarcomas remain rare tumors, the small patient cohort precludes the generalization of imaging features identified in this study. Larger studies are further needed to evaluate the imaging features of these entities to confirm common features. Due to the retrospective nature of the study, the imaging techniques were different across patients, possibly impacting the imaging

characteristics of the sarcomas. Additionally, only one reader evaluated the imaging features. With different readers, the results of the imaging features may have been different.

In conclusion, two common subgroups of undifferentiated round cell tumors with unique genetic rearrangement, CIC-DUX4 and BCOR-CCNB3, are increasingly recognized entities with similar patient demographics and imaging overlap with extraskeletal Ewing sarcoma and skeletal Ewing sarcoma. At imaging, undifferentiated round cell sarcomas with CIC-DUX4 translocations often presents as necrotic soft tissue masses with high metabolic rate and rarely with calcifications. Undifferentiated round cell sarcomas with BCOR-CCNB3 translocations usually arise from bones and exhibit vascularity and necrosis. The clinical behavior of CIC-DUX4 is more aggressive with a higher rate of metastases and death than BCOR-CCNB3.

Acknowledgements

The authors would like to thank Joanne Chin for her editorial support on this manuscript.

Funding:

This study was supported in part through the National Institutes of Health/National Cancer Institute Cancer Center Support Grant P30 CA008748.

References

1. Le Loarer F, Pissaloux D, Coindre JM, Tirode F, Vince DR. Update on Families of Round Cell Sarcomas Other than Classical Ewing Sarcomas. Surg Pathol Clin. 2017;10(3):587–620. [PubMed: 28797504]
2. Carter CS, Patel RM. Important Recently Characterized Non-Ewing Small Round Cell Tumors. Surg Pathol Clin. 2019;12(1):191–215. [PubMed: 30709443]
3. Yoshida A, Goto K, Kodaira M, Kobayashi E, Kawamoto H, Mori T, et al.CIC-rearranged Sarcomas: A Study of 20 Cases and Comparisons With Ewing Sarcomas. Am J Surg Pathol. 2016;40(3):313–23. [PubMed: 26685084]
4. Lokuhetty D, White VA, Cree IA. World Health Organization Classification of Tumours: Soft Tissue and Bone Tumours. 5 ed.Argonay, France: International Agency for Research on Cancer (IARC); 2020.
5. Antonescu CR, Owosho AA, Zhang L, Chen S, Deniz K, Huryn JM, et al.Sarcomas With CIC-rearrangements Are a Distinct Pathologic Entity With Aggressive Outcome: A Clinicopathologic and Molecular Study of 115 Cases. Am J Surg Pathol. 2017;41(7):941–9. [PubMed: 28346326]
6. Puls F, Niblett A, Marland G, Gaston CL, Douis H, Mangham DC, et al.BCOR-CCNB3 (Ewing-like) sarcoma: a clinicopathologic analysis of 10 cases, in comparison with conventional Ewing sarcoma. Am J Surg Pathol. 2014;38(10):1307–18. [PubMed: 24805859]
7. Kao YC, Owosho AA, Sung YS, Zhang L, Fujisawa Y, Lee JC, et al.BCOR-CCNB3 Fusion Positive Sarcomas: A Clinicopathologic and Molecular Analysis of 36 Cases With Comparison to Morphologic Spectrum and Clinical Behavior of Other Round Cell Sarcomas. Am J Surg Pathol. 2018;42(5):604–15. [PubMed: 29300189]
8. Lodwick GS, Wilson AJ, Farrell C, Virtama P, Smeltzer FM, Dittrich F. Estimating rate of growth in bone lesions: observer performance and error. Radiology. 1980;134(3):585–90. [PubMed: 6986621]
9. Maheshwari AV, Cheng EY. Ewing sarcoma family of tumors. J Am Acad Orthop Surg. 2010;18(2):94–107. [PubMed: 20118326]
10. Cohen-Gogo S, Cellier C, Coindre JM, Mosseri V, Pierron G, Guillemet C, et al.Ewing-like sarcomas with BCOR-CCNB3 fusion transcript: a clinical, radiological and pathological retrospective study from the Société Française des Cancers de L'Enfant. Pediatr Blood Cancer. 2014;61(12):2191–8. [PubMed: 25176412]

11. Applebaum MA, Worch J, Matthay KK, Goldsby R, Neuhaus J, West DC, et al.Clinical features and outcomes in patients with extraskeletal Ewing sarcoma. Cancer. 2011;117(13):3027–32. [PubMed: 21692057]
12. Whelan J, Hackshaw A, McTiernan A, Grimer R, Spooner D, Bate J, et al.Survival is influenced by approaches to local treatment of Ewing sarcoma within an international randomised controlled trial: analysis of EICESS-92. Clin Sarcoma Res. 2018;8:6. [PubMed: 29610659]
13. Somarouthu BS, Shinagare AB, Rosenthal MH, Tirumani H, Hornick JL, Ramaiya NH, et al.Multimodality imaging features, metastatic pattern and clinical outcome in adult extraskeletal Ewing sarcoma: experience in 26 patients. Br J Radiol. 2014;87(1038):20140123. [PubMed: 24734938]
14. Murphey MD, Senchak LT, Mambalam PK, Logie CI, Klassen-Fischer MK, Kransdorf MJ. From the radiologic pathology archives: ewing sarcoma family of tumors: radiologic-pathologic correlation. Radiographics. 2013;33(3):803–31. [PubMed: 23674776]
15. Angervall L, Enzinger FM. Extraskeletal neoplasm resembling Ewing's sarcoma. Cancer. 1975;36(1):240–51. [PubMed: 1203852]
16. Soule EH, Newton W, Moon TE, Tefft M. Extraskeletal Ewing's sarcoma: a preliminary review of 26 cases encountered in the Intergroup Rhabdomyosarcoma Study. Cancer. 1978;42(1):259–64. [PubMed: 667797]
17. Mar WA, Taljanovic MS, Bagatell R, Graham AR, Speer DP, Hunter TB, et al.Update on imaging and treatment of Ewing sarcoma family tumors: what the radiologist needs to know. J Comput Assist Tomogr. 2008;32(1):108–18. [PubMed: 18303298]
18. Reinus WR, Gehan EA, Gilula LA, Nesbit M. Plain radiographic predictors of survival in treated Ewing's sarcoma. IESS Committee. Skeletal Radiol. 1992;21(5):287–91. [PubMed: 1502579]
19. Javery O, Krajewski K, O'Regan K, Kis B, Giardino A, Jagannathan J, et al.A to Z of extraskeletal Ewing sarcoma family of tumors in adults: imaging features of primary disease, metastatic patterns, and treatment responses. AJR Am J Roentgenol. 2011;197(6):W1015–22. [PubMed: 22109315]
20. Raciborska A, Bilska K, Drabko K, Michalak E, Chaber R, Pogorzala M, et al.Response to chemotherapy estimates by FDG PET is an important prognostic factor in patients with Ewing sarcoma. Clin Transl Oncol. 2016;18(2):189–95. [PubMed: 26250765]
21. Huh J, Kim KW, Park SJ, Kim HJ, Lee JS, Ha HK, et al.Imaging Features of Primary Tumors and Metastatic Patterns of the Extraskeletal Ewing Sarcoma Family of Tumors in Adults: A 17-Year Experience at a Single Institution. Korean J Radiol. 2015;16(4):783–90. [PubMed: 26175577]
22. O'Keeffe F, Lorigan JG, Wallace S. Radiological features of extraskeletal Ewing sarcoma. Br J Radiol. 1990;63(750):456–60. [PubMed: 2379070]
23. Bharucha P, Harvilla N, White R, Papadimitriou J, Ng V, Mulligan M. Unusual distal tibia BCOR sarcoma: A case report and review of imaging features. J Clin Med Case Reports; 2019.
24. Henninger B, Glodny B, Rudisch A, Trieb T, Loizides A, Putzer D, et al.Ewing sarcoma versus osteomyelitis: differential diagnosis with magnetic resonance imaging. Skeletal Radiol. 2013;42(8):1097–104. [PubMed: 23685708]
25. Potratz J, Dirksen U, Jürgens H, Craft A. Ewing sarcoma: clinical state-of-the-art. Pediatr Hematol Oncol. 2012;29(1):1–11. [PubMed: 22295994]
26. Balamuth NJ, Womer RB. Ewing's sarcoma. Lancet Oncol. 2010;11(2):184–92. [PubMed: 20152770]

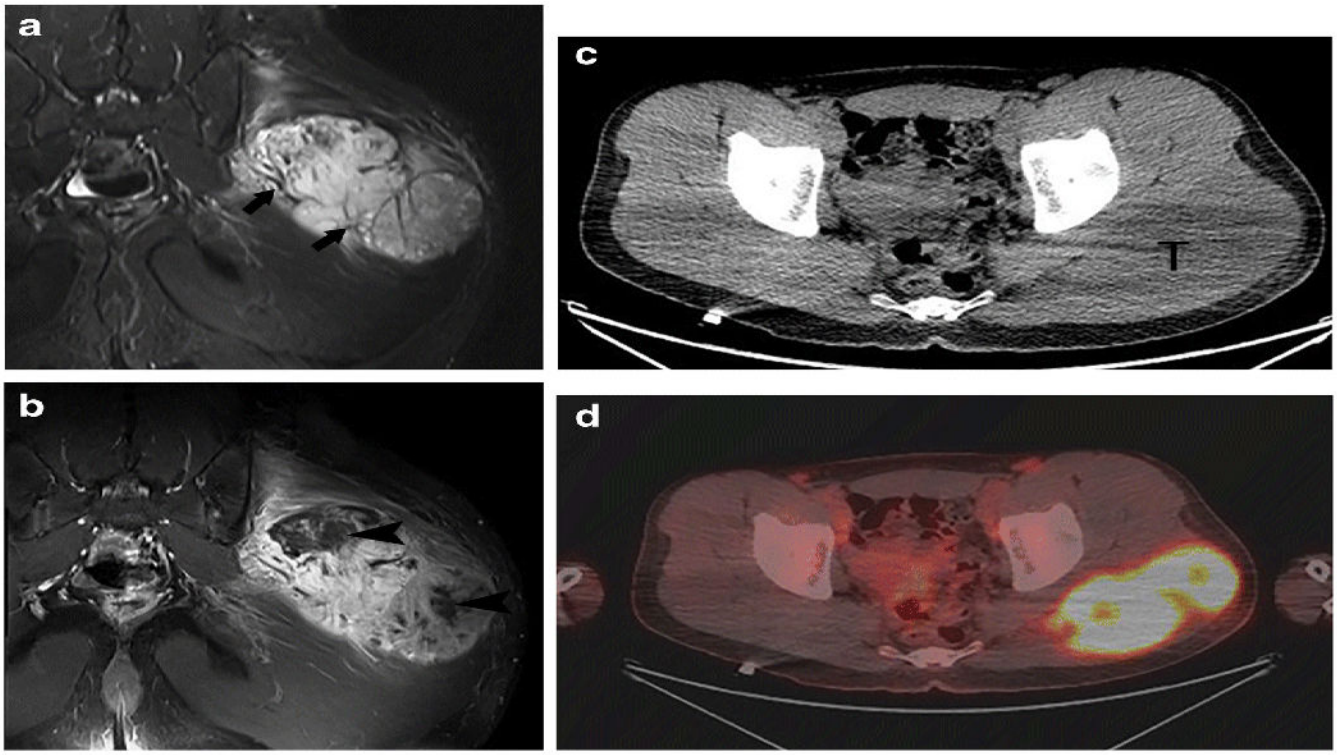

Fig. 1.

A 17-year-old man with a CIC-DUX4 tumor in the left gluteus maximus muscle. Coronal Short-TI Inversion Recovery (STIR) (a) and coronal T1-weighted fat-suppressed post-contrast (b) images show a tumor with a well-defined border and multiple linear and punctate flow voids (arrows) suggestive of vascularity. The tumor shows heterogenous contrast enhancement and necrosis (arrowheads). The tumor (T) demonstrates low attenuation on non-contrast CT (c) and is FDG-avid with SUVmax 11.1 on PET/CT (d).

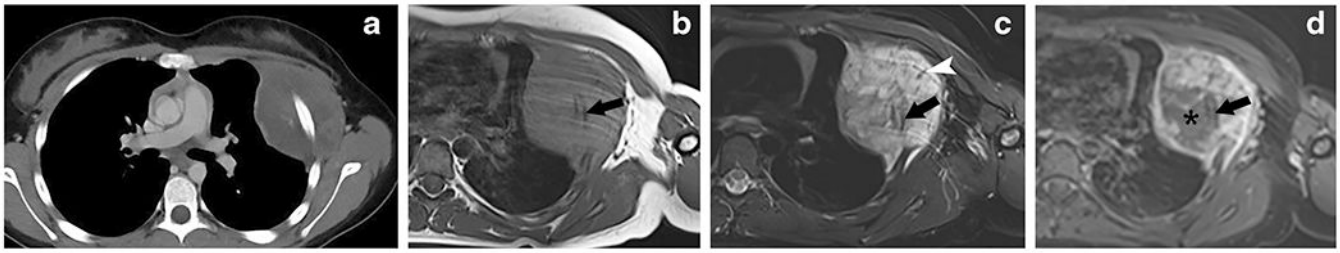

Fig. 2.

A 12-year-old girl with a CIC-DUX4 tumor in her left 3rd rib, mimicking an Askin tumor. Axial CT image (a) shows a rib lesion with a well-circumscribed soft tissue mass. Axial T1-weighted (b) and T2-weighted (c) images demonstrate medullary involvement by the tumor (arrows). Axial T1-weighted fat-suppressed post-contrast (d) image shows heterogenous contrast enhancement with necrosis (asterisk). Vascularity in the tumor is evidenced by low signal foci (arrowhead).

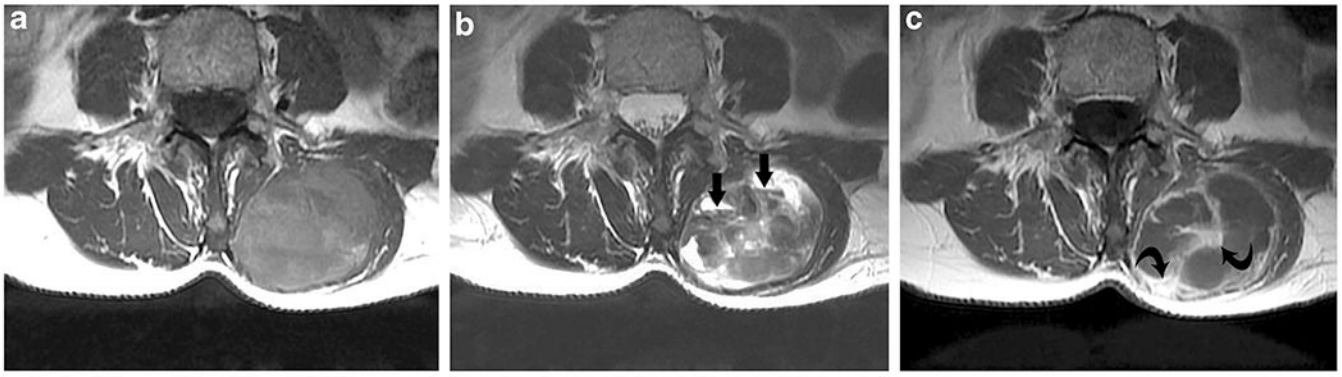

Fig. 3.

A 58-year-old woman with a CIC-DUX4 tumor in her left paraspinal musculature. Axial T1-weighted (a) and T2-weighted (b) images show an intramuscular tumor containing multiple fluid levels (arrows) and high T1 and T2 signal suggestive of hemorrhage. Axial T1-weighted fat-suppressed post-contrast image (c) shows peripheral and internal septal contrast enhancement (curved arrows) in the intramuscular tumor.

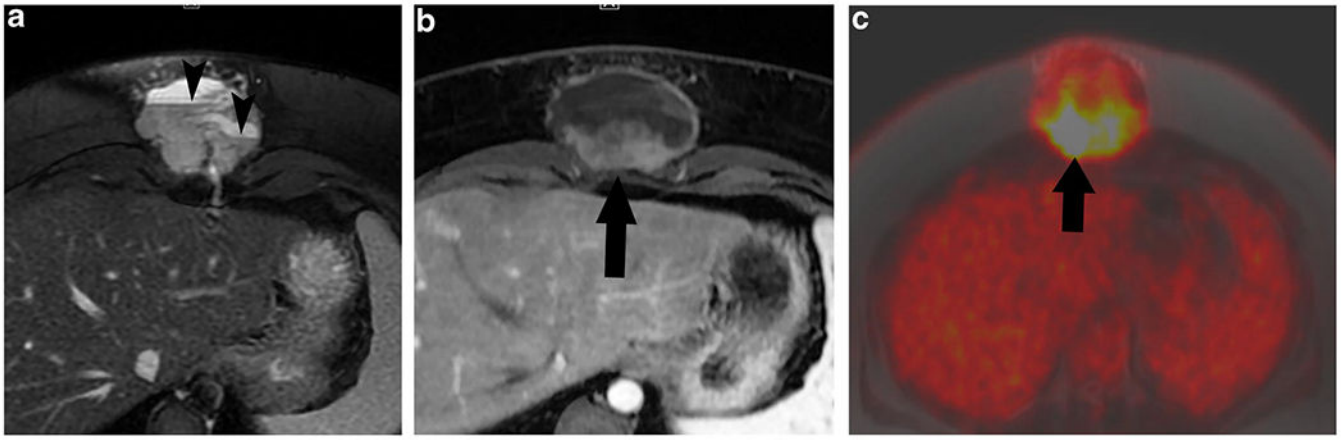

Fig. 4.

A 21-year-old woman with a CIC-DUX4 tumor in the anterior abdominal wall. Axial T2-weighted image (a) shows a subcutaneous mass containing multiple fluid levels (arrowheads) compressing on the muscles. Axial T1-weighted fat-suppressed post-contrast image (b) shows an enhancing posterior component (arrow). Axial fused PET-MRI image (c) shows FDG avidity with SUVmax measuring 5.1 in the solid component.

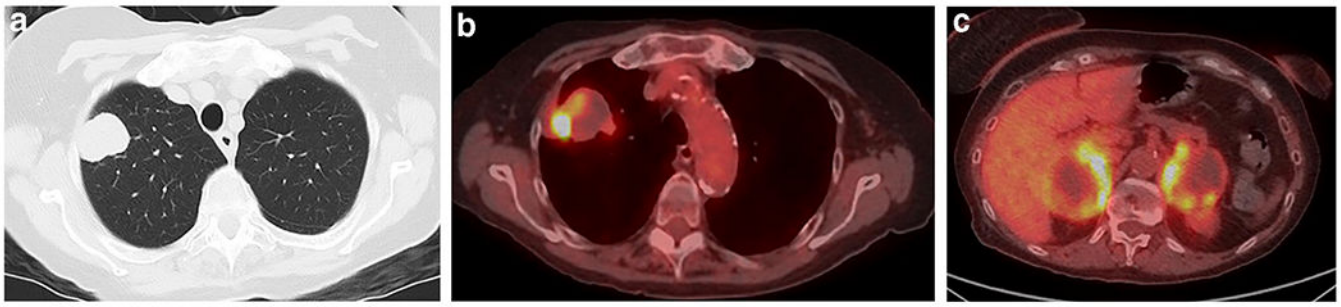

Fig. 5.

A 75-year-old woman with a CIC-DUX4 tumor in the right upper lobe with bilateral adrenal glands mimicking a primary lung cancer. Axial CT image (a) shows a well-defined right upper lobe mass. Axial fused PET-CT images (b, c) show that the mass and adrenal metastases are heterogeneously FDG avid with SUVmax measuring 18.1 in the lung mass, 9.3 in the right adrenal mass, and 7.1 in the left adrenal mass.

Fig. 6.

An 8-year-old boy with a BCOR-CCNB3 tumor in his right proximal femur. AP scout view of PET (a) shows a right femoral permeative lytic lesion (arrows) with cortical thickening (arrowhead). On an axial PET image (b), the lesion is lytic with cortical thinning (arrowheads) and periosteal reaction (curved arrow) with a soft tissue mass (T). On a PET MIP image (c), the lesion is hypermetabolic at the femoral metadiaphysis with an SUVmax of 5.7 within the soft tissue mass (arrowhead) and photopenic in the femoral diaphysis (arrow). On a coronal STIR image (d), the lesion is in the proximal femoral

metadiaphysis and diaphysis (arrows) with a soft tissue mass (arrowhead). On an axial T1-weighted fat-suppressed post-contrast image (e), the tumor shows heterogenous contrast enhancement with non-enhancing areas (arrowheads) and the soft tissue mass (T) extends beyond the periosteum (arrows).

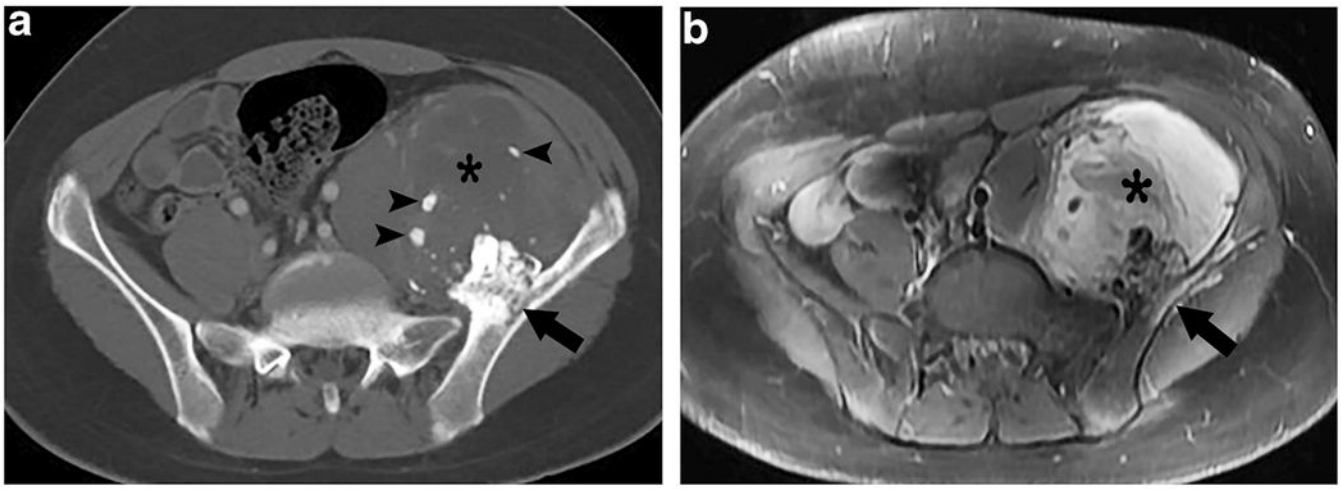

Fig. 7.

A 14 year-old-boy with a BCOR-CCNB3 tumor in left ilium. Axial CT image (a) shows a partially calcified left iliac mass (arrow) with a soft tissue mass (*) containing few small calcifications (arrowheads). Axial T1-weighted fat-suppressed post-contrast image (b) shows the enhancing intraosseous tumor (arrow) and soft tissue mass with a non-enhancing area suggestive of necrosis (*).

Table 1.

Clinical and Imaging Features of CIC-DUX4 Positive Tumors

MRI (n=10)		**n**	**%**
	Contrast enhancement	10/10	100%
	Perilesional edema	8/10	80%
	Necrosis	10/10	100%
	Flow voids	6/10	60%
	Hemorrhage	5/10	50%
	Fluid-fluid levels	2/10	20%
CT (n=7)		**n**	**%**
	Isodense to hypodense attenuation	7/7	100%
	Osseous erosions	2/7	29%
	Soft tissue calcifications	0/7	0%
FDG-PET (n=5)		**n**	**%**
	Metabolically active	5/5	100%
	Mean SUVmax	13.2 (range, 8.5-18.1)	

Table 2.

Imaging Features of BCOR-CCNB3 Positive Tumors (n=5)

Radiographs/CT (n=5)		**n**	**%**
	Lytic	2/5	40%
	Permeative	2/2	100%
	Moth-eaten	0/2	0%
	Geographic	0/2	0%
	Sclerotic	3/5	60%
	Periosteal reaction	5/5	100%
	Lamellated	3/5	60%
	Sunburst	2/5	40%
	Soft tissue calcifications	2/5	40%
MRI (n=3)		**n**	**%**
	Contrast enhancement	3/3	100%
	Flow voids	1/3	33%
	Necrosis	2/3	67%
	Perilesional Edema	2/3	67%
FDG-PET (n=3)		**n**	**%**
	Metabolically active	2/3	67%
	Mean SUVmax	6.3 (range 5.7 – 6.9)	

Table 3.

Similarities and differences of imaging findings between CIC-DUX4 and BCOR-CCNB3 tumors and Ewing sarcoma

		CIC-DUX4 (n=12)	Extraskeletal Ewing	BCOR-CCNB3 (n=5)	Skeletal Ewing
MRI					
	Contrast enhancement	100%	73.7%–100%	100%	100%
	Necrosis	100%	82%	66%	72%
	Flow voids	60%	90%	66%	*
	Hemorrhage	50%	19%	0%	*
Radiographs/CT					
	Lytic	8%	-	40%	60%
	Sclerotic	0%	-	60%	32%–40%
	Periosteal Reaction	8%	-	100%	58%–84%
	Isodense to hypodense attenuation	100%	73%	100%	98%
	Soft tissue calcifications	0%	0%–25%	40%	7%–9%
FDG-PET (n=5)					
	Mean SUVmax	13.2 (8.5–8.1)	5-7	6.3 (5.7–6.9)	5.3–11.3

*Exact percentiles not well validated in the literature

- Not applicable due to lack of bony involvement